

# Atomically inspired $k \cdot p$ approach and valley Zeeman effect in transition metal dichalcogenide monolayers

D. V. Rybkovskiy

*A. M. Prokhorov General Physics Institute, RAS, 38 Vavilov street, 119991, Moscow, Russia*

I. C. Gerber

*Université de Toulouse, INSA-CNRS-UPS, LPCNO, 135 Ave. de Rangueil, 31077 Toulouse, France*

M. V. Durnev\*

*Ioffe Institute, 194021 St. Petersburg, Russia*

(Received 9 October 2016; revised manuscript received 6 March 2017; published 6 April 2017)

We developed a six-band  $k \cdot p$  model that describes the electronic states of monolayer transition metal dichalcogenides (TMDCs) in  $\mathbf{K}$  valleys. The set of parameters for the  $k \cdot p$  model is uniquely determined by decomposing tight-binding (TB) models in the vicinity of  $\mathbf{K}^\pm$  points. First, we used TB models existing in literature to derive systematic parametrizations for different materials, including MoS<sub>2</sub>, WS<sub>2</sub>, MoSe<sub>2</sub>, and WSe<sub>2</sub>. Then, by using the derived six-band  $k \cdot p$  Hamiltonian we calculated effective masses, Landau levels, and the effective exciton  $g$ -factor  $g_{X^0}$  in different TMDCs. We showed that TB parametrizations existing in literature result in small absolute values of  $g_{X^0}$ , which are far from the experimentally measured  $g_{X^0} \approx -4$ . To further investigate this issue we derived additional sets of  $k \cdot p$  parameters for different TMDCs by developing our own TB parametrizations based on simultaneous fitting of *ab initio* calculated, within the density functional theory (DFT) and *GW* approaches, energy dispersion, and the value of  $g_{X^0}$ . We showed that the change in TB parameters, which only slightly affects the dispersion of higher conduction and deep valence bands, may result in a significant increase of  $|g_{X^0}|$ , yielding close-to-experiment values of  $g_{X^0}$ . Such a high parameter sensitivity of  $g_{X^0}$  opens a way to further improvement of the description of TMDCs electronic structures by DFT and/or TB models.

DOI: [10.1103/PhysRevB.95.155406](https://doi.org/10.1103/PhysRevB.95.155406)

## I. INTRODUCTION

Monolayers of transition metal dichalcogenides (TMDCs) have attracted recently much attention due to their exceptional properties, such as coupling of spin and valley degrees of freedom, which allows for the valley polarization with a circularly polarized light in these materials [1–6]. Recent magnetophotoluminescence experiments revealed the significant Zeeman splitting of emission lines associated with optical recombination of excitons and trions in different valleys. The effective exciton  $g$  factors of this “valley Zeeman effect” in a magnetic field directed normal to a monolayer plane were found to be  $g_{X^0} \approx -4$  for a wide range of investigated materials, including selenides [7–12], sulfides [13,14], and tellurides [15]. Theoretical calculations of exciton  $g$  factor were done in Refs. [16–18].

The electron band structure of crystalline solids is usually calculated using *ab initio* methods such as density functional theory (DFT), which requires a minimum set of input parameters and provides a rather accurate description of energy bands. This method is widely applied to calculate the band dispersion in TMDCs, however the evaluation of the  $g$  factors of charge carriers within the DFT method is difficult. On the other hand, the multiband  $k \cdot p$  method is perfectly suited for theoretical investigation of both energy dispersion in the vicinity of selected points, high-symmetry, as a rule, in the  $k$  space and

evaluation of various phenomena, such as magneto-optical and transport effects, including Zeeman effect, optical absorption, and photogalvanics [19,20]. However, this method is empirical in a sense that the parameters of the effective Hamiltonian should be found by comparison with *ab initio* calculations and/or with experiments. Despite this, the  $k \cdot p$  method is exact provided all energy bands are taken into account. Reasonable approximations, which include the set of well-selected bands that account for point symmetry of the material and are close in energy, are usually found for a variety of semiconductors (including group-IV materials, such as Si and Ge, III-V and II-VI binary compounds, including GaAs, CdTe, HgTe, and many others) [21–24].

The simple two-band  $k \cdot p$  model, which accounts for the bottom conduction and topmost valence bands, is insufficient for calculation of exciton Zeeman effect since the exciton  $g$ -factor  $g_{X^0}$  vanishes in the two-band  $k \cdot p$  approximation [11]. Therefore the development of multiband  $k \cdot p$  models is required. Several multiband  $k \cdot p$  models describing electronic spectra in TMDCs [25–27] are available in literature. In these works analytical expressions for multiband Hamiltonians are present, however, its detailed parametrization, i.e., the set of parameters describing positions of energy bands and the values of interband matrix elements of momentum operator, is not established. These multiband Hamiltonians are used only as a starting point to derive an effective two-band  $k \cdot p$  model, which includes the contributions of other bands by the perturbation theory. This procedure results in additional phenomenological terms describing contributions of remote

\*Corresponding author: [durnev@mail.ioffe.ru](mailto:durnev@mail.ioffe.ru)

bands in the two-band  $k \cdot p$  Hamiltonian. The values of these terms, i.e., quadratic and cubic in  $\mathbf{k}$  diagonal and off-diagonal terms, are found by fitting the DFT band structure in the vicinity of  $K$  points of the Brillouin zone. However, this direct parametrization of the  $k \cdot p$  Hamiltonian is ambiguous, because basically the same set of energies and effective masses can be reproduced with different values of the interband matrix elements. Moreover, as shown by DFT calculations, and as we will discuss below, the closely lying excited conduction ( $c + 2$ ) and valence ( $v - 3$ ) bands, strictly speaking, cannot be treated as remote and should be also directly included in the  $k \cdot p$  model.

In this work we obtain parametrization of the multiband  $k \cdot p$  model using an alternative approach based on the idea proposed in Ref. [11]. This approach takes the use of the tight-binding (TB) model as an intermediate step between DFT and  $k \cdot p$  modeling. Unlike the  $k \cdot p$  method the TB model provides the electronic band structure in the whole Brillouin zone. By decomposing the TB Hamiltonian in the vicinity of a given wave vector in the Brillouin zone, we obtain a multiband  $k \cdot p$  Hamiltonian (the number of bands is equal to the number of atomic orbitals included in the TB model) with a set of parameters that are uniquely determined by the TB parametrization. Such a procedure gives an unambiguous set of  $k \cdot p$  parameters, which is explicitly related to a given TB model. In contrast to existing two-band  $k \cdot p$  models the derived multiband Hamiltonian allows us to analyze the contributions of different bands to exciton  $g$  factor and thus establish importance of these bands for other physical problems that can be solved within the  $k \cdot p$  method.

On the other hand, the TB models still require the selection of parameters, because, just like in  $k \cdot p$  approach, it turns out that fitting just the band dispersion is not sufficient to obtain a single unequivocal set of parameters. Additional values, such as the weights of atomic orbitals in TB wave function decomposition, are used to constrict possible parametrizations. In this work we use the experimentally measured value of exciton  $g$  factor as an additional constraint to improve the TB parametrization. Such an approach has proven itself for classical semiconductors like GaAs, where the  $k \cdot p$  model has been improved particularly by taking into account the experimentally measured electron  $g$  factors [28].

As a starting point we use several existing 11-band TB models [29–33]. These models include  $d$ -type orbitals of metal atoms and  $p$ -type orbitals of chalcogen atoms, and capture all symmetries of the studied system. The resulting  $k \cdot p$  Hamiltonian contains six closely lying bands (including the topmost valence and bottom conduction bands) that have even parity with respect to mirror reflection in the monolayer plane and properly describes  $C_{3h}$  point symmetry of  $K$  valleys. We present a systematic parametrization of the six-band  $k \cdot p$  Hamiltonian by expansion of TB Hamiltonians [29–33] in the vicinity of  $K^\pm$  points of the Brillouin zone for different materials ( $\text{MoS}_2$ ,  $\text{WS}_2$ ,  $\text{MoSe}_2$ ,  $\text{WSe}_2$ ) and different TB models. We also do the whole three-step procedure on our own, i.e., perform post-DFT calculations by applying  $GW$  formalism to obtain reliable band gaps and accurate band dispersion, fit it with the TB model, and do the  $k \cdot p$

decomposition, which allows us, as a result, to obtain an independent  $k \cdot p$  parametrization. In previous studies the main focus was made on DFT calculations using mainly local or semilocal exchange-correlation functionals [29–31], whereas a hybrid functional was also used [32] to partially correct the severe underestimation of band gap values usually observed at the DFT level for  $\text{MoS}_2$  monolayers, see Ref. [34] for a recent review. The use of  $GW$  correction strongly affects the effective charge carrier masses [35,36] too. In Ref. [31] TB parameters were extracted from  $GW$  calculations for  $\text{MoS}_2$  and were used to correct parameters extracted from standard DFT electronic structures.

Then we use the derived six-band  $k \cdot p$  Hamiltonian to calculate effective masses, Landau levels, and the effective exciton  $g$ -factor  $g_{X^0}$  in different TMDCs. We establish that the main contributions to  $g_{X^0}$  result from the mixing with excited conduction ( $c + 2$ ) and deep valence ( $v - 3$ ) bands. We show that the calculated values of  $g_{X^0}$  and effective masses vary in a wide range for different TB parametrizations. The wide spread of calculated  $g_{X^0}$  indicates ambiguity of the available TB parametrizations. Moreover, the calculated values of  $g_{X^0}$  available in literature TB models ( $|g_{X^0}| \lesssim 1$ ) are rather far from experimental values. To overcome this problem, we find our own TB parametrizations based on the simultaneous fitting of DFT+ $GW$  band structure and the experimental value of  $g_{X^0}$ . By decomposing the obtained TB Hamiltonians we were able to find  $k \cdot p$  parametrization sets, which well describe the experimental exciton  $g$  factor ( $g_{X^0} \approx -4$ ), as well as conduction and valence band effective masses and the wave functions coefficients. This result underlies the importance of the careful choice for the DFT starting point calculations and TB parametrizations: along with effective masses and energy gaps the  $g$ -factor value may serve as a test for improving both the DFT calculations and TB models.

## II. EFFECTIVE $k \cdot p$ HAMILTONIAN

As a starting point for construction of an effective  $k \cdot p$  Hamiltonian we use 11-band tight-binding models developed in Refs. [29–33]. These tight-binding models include three  $p$ -type orbitals on each of the two chalcogen atoms ( $X$ ) and five  $d$ -type orbitals on a metal atom ( $M$ ). The electron wave function within the tight-binding approximation is presented as a linear combination of atomic orbitals  $\phi_j^{(a)}$  [11],

$$\Psi_k^{(n)}(\mathbf{r}) = \sum_{a,l,j} e^{i\mathbf{k}\mathbf{R}_{a,l}} C_j^{(a)} \phi_j^{(a)}(\mathbf{r} - \mathbf{R}_{a,l}), \quad (1)$$

where  $n$  is a number of an electronic band,  $\mathbf{k}$  is a wave vector,  $a = M, X$  denotes the type of an atom,  $l$  runs through the atoms of a given type,  $j$  enumerates the set of orbitals,  $\mathbf{R}_{a,l}$  gives the position of atoms in a two-dimensional lattice, and  $C_j^{(a)}$  are coefficients.

The basis orbitals of the 11-band tight-binding model are [29–33]

$$\phi_j^{(a)} = \{d_{z^2}, d_+, d_-, p_+, p_-, p_{z,A}, d_{xz}, d_{yz}, p_{x,A}, p_{y,A}, p_{z,S}\}, \quad (2)$$

where  $d_\pm = d_{x^2-y^2} \pm 2id_{xy}$ ,  $p_\pm = p_{x,S} \pm ip_{y,S}$ ,  $d_\alpha$  denotes the orbital with a  $d$ -like symmetry of the  $M$  atom,  $p_{\beta,S} =$

$(p_{\beta,t} + p_{\beta,b})/\sqrt{2}$ ,  $p_{\beta,A} = (p_{\beta,t} - p_{\beta,b})/\sqrt{2}$  are the symmetric and asymmetric combinations of the  $p$ -type orbitals of the top ( $t$ ) and bottom ( $b$ ) X atoms in the unit cell,  $x$  and  $y$  axes lie in the monolayer plane, and  $z$  is the monolayer normal. The spin-orbit interaction between electron spin and orbital momenta of atomic orbitals [30,31] is neglected in this work.

If the  $z \rightarrow -z$  mirror symmetry is conserved, i.e., for a free-standing monolayer in the absence of external electric field and strain, the Hamiltonian, which describes the energy spectrum of a monolayer electron with a wave vector  $\mathbf{k}$ , written in the basis Eq. (2), has the form

$$\mathcal{H}(\mathbf{k}) = \begin{pmatrix} \mathcal{H}_E & 0 \\ 0 & \mathcal{H}_O \end{pmatrix}. \quad (3)$$

Here  $\mathcal{H}_E$  is the  $6 \times 6$  block acting on the orbitals with even with respect to  $z \rightarrow -z$  symmetry, and  $\mathcal{H}_O$  is the  $5 \times 5$  block acting on the orbitals with odd symmetry. The exact form of blocks  $\mathcal{H}_E$  and  $\mathcal{H}_O$  depends on a particular tight-binding model [29–33]. It is known that the Bloch functions of the bottom conduction and topmost valence bands, which are of the main interest in this work, are even with respect to  $z \rightarrow -z$  reflection [25,27], and therefore these bands are described by the  $\mathcal{H}_E$  block. We note that magnetic field normal to a monolayer does not break the parity of wave functions, and hence we do not need the  $\mathcal{H}_O$  block in the calculation of  $g_{X^0}$ . We also note that the mixing of the  $\mathcal{H}_E$  and  $\mathcal{H}_O$  blocks by a perturbation that breaks  $z \rightarrow -z$  symmetry does not affect  $g_{X^0}$  in the first order in this perturbation.

To construct an effective  $k \cdot p$  Hamiltonian in the vicinity of  $\mathbf{K}^\pm = (\pm 4\pi/3a_0, 0)$  points, where  $a_0$  is the lattice constant, we will decompose the tight-binding Hamiltonian  $\mathcal{H}_E(\mathbf{k})$  over a small wave vector  $\mathbf{q} = \mathbf{k} - \mathbf{K}^\pm$ . Up to the second-order terms this decomposition yields

$$\begin{aligned} \mathcal{H}_E^\pm(\mathbf{q}) &\approx \mathcal{H}_E(\mathbf{K}^\pm) + \sum_{\alpha=x,y} \frac{\partial \mathcal{H}_E}{\partial k_\alpha}(\mathbf{K}^\pm) q_\alpha \\ &+ \frac{1}{2} \sum_{\alpha,\beta=x,y} \frac{\partial^2 \mathcal{H}_E}{\partial k_\alpha \partial k_\beta}(\mathbf{K}^\pm) q_\alpha q_\beta. \end{aligned} \quad (4)$$

Electron wave functions at  $\mathbf{K}^\pm$  valleys of  $\text{MX}_2$  transform according to irreducible representations (irreps) of the  $C_{3h}$  point group. We denote six wave functions that diagonalize  $\mathcal{H}_E^\pm(\mathbf{q})$  at  $\mathbf{q} = 0$  as  $\Psi_{E_1'}^{(v-5)}$ ,  $\Psi_{A'}^{(v-4)}$ ,  $\Psi_{E_2'}^{(v-3)}$ ,  $\Psi_{A'}^{(v)}$ ,  $\Psi_{E_1'}^{(c)}$ ,  $\Psi_{E_2'}^{(c+2)}$ , where a superscript names the electronic band and a subscript denotes the corresponding irreducible representation ( $A'$ ,  $E_1'$ , and  $E_2'$ ), see Table I. Note that in addition to two conduction ( $c$  and  $c+2$ ) and two valence ( $v$  and  $v-3$ ) bands, known from the four-band  $k \cdot p$  models [25,27], the six-band model contains two deep valence bands  $v-4$  and  $v-5$ , which transform at  $\mathbf{K}^+$  point via  $A'$  and  $E_1'$  representations, respectively.

In the new basis  $\mathcal{H}_E^\pm(\mathbf{q})$  can be written as

$$\mathcal{H}_E^\pm(\mathbf{q}) = \mathcal{H}_1^\pm(\mathbf{q}) + \mathcal{H}_2^\pm(\mathbf{q}), \quad (5)$$

TABLE I. The nonzero coefficients  $C_j^{(a)}$  of wave functions Eq. (1) at  $\mathbf{K}^+$  point and corresponding irreducible representations of the  $C_{3h}$  point group. The phases of the wave functions are chosen in such a way that  $\alpha_i$  and  $\beta_i$  are real numbers,  $\alpha_i^2 + \beta_i^2 = 1$ , and  $\alpha_i > 0$ . We denote  $p_z \equiv p_{z,A}$ .

Irrep	Band	Nonzero wave function coefficients
$A'$	$v, v-4$	$\Psi^{(v)}: C_{d_+} = \alpha_1, C_{p_+} = i\beta_1;$ $\Psi^{(v-4)}: C_{d_+} = \beta_1, C_{p_+} = -i\alpha_1$
$E_1'$	$c, v-5$	$\Psi^{(c)}: C_{d_{z^2}} = \alpha_2, C_{p_-} = i\beta_2;$ $\Psi^{(v-5)}: C_{d_{z^2}} = \beta_2, C_{p_-} = -i\alpha_2$
$E_2'$	$c+2, v-3$	$\Psi^{(c+2)}: C_{d_-} = \alpha_3, C_{p_z} = \beta_3;$ $\Psi^{(v-3)}: C_{d_-} = \beta_3, C_{p_z} = -\alpha_3$

where the first term contains linear in  $\mathbf{q}$  terms:

$$\mathcal{H}_1^+(\mathbf{q}) = \begin{pmatrix} E_{v-5} & \delta_7 q_- & \delta_6 q_+ & \delta_4 q_- & 0 & \delta_2 q_+ \\ \delta_7 q_+ & E_{v-4} & \delta_5 q_- & 0 & \delta_3 q_+ & \delta_1 q_- \\ \delta_6 q_- & \delta_5 q_+ & E_{v-3} & \gamma_2 q_+ & \gamma_5 q_- & 0 \\ \delta_4 q_+ & 0 & \gamma_2 q_- & E_v & \gamma_3 q_+ & \gamma_4 q_- \\ 0 & \delta_3 q_- & \gamma_5 q_+ & \gamma_3 q_- & E_c & \gamma_6 q_+ \\ \delta_2 q_- & \delta_1 q_+ & 0 & \gamma_4 q_+ & \gamma_6 q_- & E_{c+2} \end{pmatrix}, \quad (6)$$

and the second one

$$[\mathcal{H}_2^\pm(\mathbf{q})]_{nl} = \frac{\hbar^2 q^2}{2m_n'} \delta_{nl}, \quad n, l = 1, \dots, 6 \quad (7)$$

is a diagonal matrix with quadratic in  $\mathbf{q}$  elements. In Eqs. (6) and (7)  $E_n$  ( $n = c+2, c, \dots$ ) are the band energies at  $\mathbf{K}^\pm$  points,  $\gamma_j$  and  $\delta_j$  are parameters,  $q_\pm = q_x \pm iq_y$ , and  $q^2 = q_x^2 + q_y^2$ . The effective masses  $m_n'$  describe contributions to the band dispersion arising from the mixing with remote bands, which are not present in the  $k \cdot p$  model [11]. Note that in the decomposition of the off-diagonal elements of the tight-binding Hamiltonian (4) we retain only the linear in  $\mathbf{q}$  terms. The phases of wave functions at  $\mathbf{K}^+$  point (Table I) are chosen in such a way that parameters  $\gamma_j$  and  $\delta_j$  are real. Parameters of the  $k \cdot p$  Hamiltonians (6) and (7) for different parametrizations, materials, and tight-binding models are listed in Tables IV and V of Appendix A.

To derive the  $k \cdot p$  Hamiltonian  $\mathcal{H}_1^-$  at the  $\mathbf{K}^-$  point of the Brillouin zone one should replace  $q_+$  by  $q_-$  and vice versa in Eq. (6) [37]. Note that at  $\mathbf{k} = \mathbf{K}^-$  basis wave functions  $\Psi^{(c)}$  and  $\Psi^{(v-5)}$  transform according to  $E_2'$  irreducible representation, whereas  $\Psi^{(c+2)}$  and  $\Psi^{(v-3)}$  transform according to  $E_1'$ .

The effective masses of the main conduction and valence bands in the framework of  $k \cdot p$  model are

$$\frac{1}{m_c} = \frac{1}{m_c'} + \frac{1}{m_c^*}, \quad \frac{1}{m_v} = \frac{1}{m_v'} + \frac{1}{m_v^*}, \quad (8)$$

where

$$\begin{aligned} \frac{1}{m_c^*} &= \frac{2}{\hbar^2} \left( \frac{\gamma_5^2}{E_c - E_{v-3}} + \frac{\gamma_3^2}{E_c - E_v} \right. \\ &\left. + \frac{\gamma_6^2}{E_c - E_{c+2}} + \frac{\delta_3^2}{E_c - E_{v-4}} \right), \end{aligned} \quad (9)$$

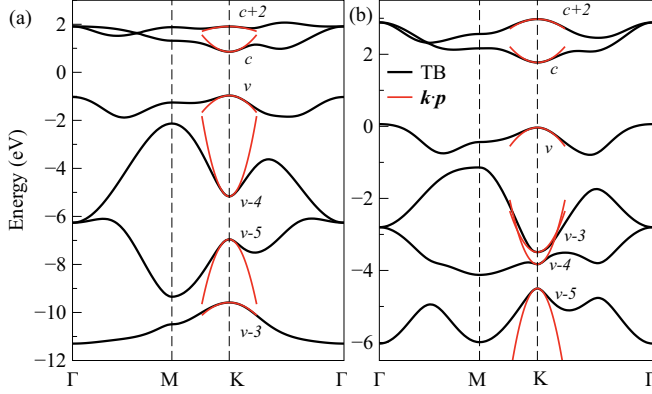


FIG. 1. Electronic spectra of MoS<sub>2</sub> calculated using TB models Rostami *et al.* [33] (a) and Fang *et al.* [31] (b). Red lines are  $k \cdot p$  quadratic dispersions at  $\mathbf{K}$  point calculated using effective masses for each band (see text for details). Note the different order of deep valence bands in two panels.

$$\frac{1}{m_v^*} = \frac{2}{\hbar^2} \left( \frac{\gamma_2^2}{E_v - E_{v-3}} + \frac{\gamma_3^2}{E_v - E_c} + \frac{\gamma_4^2}{E_v - E_{c+2}} + \frac{\delta_4^2}{E_v - E_{v-5}} \right) \quad (10)$$

result from the mixing of electronic bands described by Hamiltonian (6), whereas  $m_c'$  and  $m_v'$  account for the mixing with remote bands, see Eq. (7).

Figure 1 shows the dispersion of electronic bands in MoS<sub>2</sub> calculated in the framework of TB models of Refs. [31,33], respectively, in Figs. 1(b) and 1(a) and the dispersion  $\varepsilon_n = E_n + \hbar^2 q^2 / 2m_n$ , where an effective mass of the  $n$ th band is calculated similar to  $n = c$  and  $n = v$ , see Eqs. (8)–(10). Figure 1 illustrates that a certain care should be taken when labeling the valence bands: the bands are labeled according to its wave functions representations, see Table I, and the order might be different for different TB models.

The effective masses  $m_c$  and  $m_v$  for different TB models are listed in Tables II and III. Agreements with previous studies [25] and experimental estimates of  $m_v$  values [38] are indeed good, providing a good basis for  $g$ -factors determination. As for  $m_c$  values the TB parametrizations obtained in this work fit the local maximum in the conduction band in the  $K$ - $\Gamma$

TABLE II. The values of  $g$  factors and effective masses (in units of  $m_0$ ) of the  $v$  and  $c$  bands calculated within the  $k \cdot p$  model from different TB parametrizations (listed in footnotes) based on DFT calculations.

	MoS <sub>2</sub> <sup>a</sup>	MoS <sub>2</sub> <sup>b</sup>	MoSe <sub>2</sub> <sup>b</sup>	WS <sub>2</sub> <sup>b</sup>	WSe <sub>2</sub> <sup>b</sup>
$m_v$	-0.54	-0.72	-0.82	-0.53	-0.57
$m_c$	0.54	0.86	1.02	0.68	0.76
$g_v$	8.73	5.57	5.12	6.08	5.64
$g_c$	7.82	5.41	5.12	6.13	5.79
$g_{X^0} = g_c - g_v$	-0.91	-0.16	0	0.05	0.15

<sup>a</sup>TB model of Ref. [33] based on DFT calculations.

<sup>b</sup>TB model of Ref. [31] based on DFT calculations.

TABLE III. The values of  $g$  factors and effective masses (in units of  $m_0$ ) of the  $v$  and  $c$  bands calculated within the  $k \cdot p$  model from different TB parametrizations (listed in footnotes) based on DFT+ $GW$  calculations.

	MoS <sub>2</sub> <sup>a</sup>	MoS <sub>2</sub> <sup>b</sup>	MoS <sub>2</sub> <sup>c</sup>	MoSe <sub>2</sub> <sup>c</sup>	WS <sub>2</sub> <sup>c</sup>	WSe <sub>2</sub> <sup>c</sup>
$m_v$	-0.58	-0.40	-0.56	-0.57	-0.49	-0.58
$m_c$	0.90	0.37	0.37	0.52	0.40	0.46
$g_v$	6.18	11.90	5.59	5.83	5.96	4.08
$g_c$	6.83	10.15	1.77	3.21	2.11	0.24
$g_{X^0} = g_c - g_v$	0.65	-1.75	-3.82	-2.62	-3.85	-3.84

<sup>a</sup>TB model of Ref. [31] based on DFT+ $GW$  calculations.

<sup>b</sup>DFT+ $GW$  and TB parametrization of this work (TB model based on Ref. [33]).

<sup>c</sup>DFT+ $GW$  and TB parametrization of this work (TB model based on Ref. [31]).

direction, see Fig. 3, and give  $m_c$  values close to the ones in DFT+ $GW$  calculations.

### III. ZEEMAN EFFECT

In this section we use the developed  $k \cdot p$  model to calculate the  $g$  factors of electrons in conduction and valence bands. The main interest, however, is related to the exciton  $g$  factor, which has been measured in a number of recent experiments by optical means. Single carrier Zeeman splittings can be determined, for instance, from the measurements of Shubnikov–de Haas oscillations.

We consider the Zeeman splitting of electrons in  $\mathbf{K}^\pm$  valleys in magnetic field  $\mathbf{B} = (0, 0, B_z)$  perpendicular to a monolayer plane. The Zeeman effect contains spin and valley contributions described by  $g$ -factors  $g_0$  and  $g_{\text{orb}}$ , respectively,

$$\mathcal{H}_B = \frac{g_0}{2} \mu_B B_z \sigma_z + \frac{g_{\text{orb}}}{2} \mu_B B_z \tau_z. \quad (11)$$

Here  $\sigma_z$  is a spin operator ( $\sigma_z = \pm 1$  for spin-up and spin-down electrons, respectively),  $\tau_z$  represents the valley degree of freedom ( $\tau_z = \pm 1$  for  $\mathbf{K}^+$  and  $\mathbf{K}^-$  electrons, respectively), and  $\mu_B$  is the Bohr magneton. The effective  $g$  factors of  $\mathbf{K}^+$  and  $\mathbf{K}^-$  electrons are defined as [11]

$$g_{c,v}^{\mathbf{K}^+} \equiv g_{c,v} = g_0 + g_{\text{orb}}^{c,v}, \quad g_{c,v}^{\mathbf{K}^-} = -g_{c,v}^{\mathbf{K}^+}. \quad (12)$$

The valley term  $g_{\text{orb}}^{c,v}$  has an orbital nature and accounts for the mixing of the electronic bands by magnetic field. Within the  $k \cdot p$  scheme this mixing is obtained by replacing  $\mathbf{q}$  in Eq. (6) with  $\mathbf{q} - (e/\hbar c)\mathbf{A}$ , where  $e = -|e|$  is the electron charge, and  $\mathbf{A}$  is the vector potential of the magnetic field, resulting in (cf. Ref. [11])

$$g_{c,v}^{\text{orb}} = \frac{4m_0}{\hbar^2} \left( -\frac{\gamma_5^2}{E_c - E_{v-3}} + \frac{\gamma_3^2}{E_c - E_v} - \frac{\gamma_6^2}{E_c - E_{c+2}} + \frac{\delta_3^2}{E_c - E_{v-4}} \right), \quad (13)$$

$$g_{v}^{\text{orb}} = \frac{4m_0}{\hbar^2} \left( \frac{\gamma_2^2}{E_v - E_{v-3}} - \frac{\gamma_3^2}{E_v - E_c} + \frac{\gamma_4^2}{E_v - E_{c+2}} - \frac{\delta_4^2}{E_v - E_{v-5}} \right). \quad (14)$$

The spin  $g$ -factor  $g_0$  comprises two contributions, namely, the bare electron  $g$  factor ( $g_0 = 2$ ) and a small contribution due to the spin-orbit interaction, which is not taken into account in our model. This contribution within the  $k \cdot p$  model is of the order of  $\sim g_{\text{orb}} \Delta_{\text{so}} / \Delta E_{ij} \ll g_{\text{orb}}$ , where  $\Delta_{\text{so}}$  is the spin-orbit splitting of a given band, and  $\Delta E_{ij}$  is a characteristic energy distance to other bands.

The  $\sigma^+$  and  $\sigma^-$  photoluminescence lines observed in experiments originate from the radiative recombination of neutral excitons  $X^0$  with electrons occupying  $K^+$  and  $K^-$  valleys, respectively [39]. Therefore the effective Zeeman splitting of  $X^0$  is  $\Delta_Z = g_{X^0} \mu_B B_z$  with [11]

$$g_{X^0} = g_c - g_v. \quad (15)$$

In this difference, according to Eqs. (12)–(14), the contribution to  $g_c$  and  $g_v$ , which occurs due to the mixing between  $c$  and  $v$  bands ( $\propto \gamma_3^2$ ), cancels out, so that nonzero contributions to  $g_{X^0}$  arise due to the mixing of  $v$  and  $c$  with deep valence and excited conduction bands.

#### IV. DISCUSSION

Tables II and III present the values of  $g$  factors and effective masses calculated within the developed  $k \cdot p$  model after Eqs. (13) and (14) and Eqs. (8)–(10). Since the large contributions to  $g_c$  and  $g_v$  that originate from the mixing between  $v$  and  $c$  bands cancel out in the exciton  $g$  factor, the value of  $g_{X^0}$  is defined by the mixing with deep valence and excited conduction bands. The main contributions to  $g_{X^0}$  in the studied parametrizations come from the mixing with  $v - 3$  and  $c + 2$  bands, i.e., from the terms  $-\gamma_5^2 / (E_c - E_{v-3})$  and  $-\gamma_6^2 / (E_c - E_{c+2})$  in Eq. (13) and terms  $\gamma_2^2 / (E_v - E_{v-3})$  and  $\gamma_4^2 / (E_v - E_{c+2})$  in Eq. (14). As an example, the contribution from  $c + 2$  gives  $\approx 15\%$  of the total  $g_c$  value, and the contribution from  $v - 3$  gives  $\approx 30\%$  of the total  $g_v$  value for MoS<sub>2</sub> parametrization (a) in Table II. As seen from Table II, existing in literature TB models result in small absolute values of  $g_{X^0}$ , which are far from the experimentally measured  $g_{X^0} \approx -4$ .

Based on our own DFT and post-DFT ( $GW$ ) calculations and TB fitting procedure (see computational details and dispersion of energy bands in Appendixes B and C) we obtained additional  $k \cdot p$  parametrizations for MoS<sub>2</sub>, WS<sub>2</sub>, MoSe<sub>2</sub>, and WSe<sub>2</sub>, see columns b–f in Tables III and V. For this purpose we use two different TB models, the 11-parameters TB model of Ref. [33] and the TB model of Ref. [31] with 25 independent parameters. Within the fitting procedure we numerically extract parameters of the  $k \cdot p$  Hamiltonian and calculate exciton  $g$  factor using Eqs. (13)–(15). We then use the value of  $g_{X^0}$  as an extra fitting parameter (we fit it to the experimental value  $g_{X^0} \approx -4$ ) additional to band dispersions and wave function coefficients. Equations (13)–(15) use single-particle electron and hole  $g$  factors at bands extrema and do not take into account the renormalization of  $g_{X^0}$  due to the Coulomb effect. Although this renormalization, as will be shown below, might be significant, it is still not sufficient to explain experimentally observed large values of  $g_{X^0}$ , if we start from the available in literature TB parametrizations, which give  $g_c - g_v \approx 0$ . Therefore it is more likely that the large experimental values of exciton

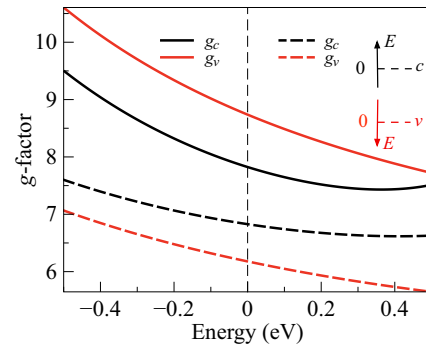


FIG. 2. Conduction and valence band  $g$ -factors  $g_c$  and  $g_v$  as functions of electron and hole energy, respectively. The energies are counted from the bottom of the conduction band and from the top of the valence band as shown in the inset. The solid and dashed lines show results of calculations for parametrization (a) from Table IV and parametrization (a) from Table V, respectively.

$g$  factor are related to the renormalization of single-particle  $g$  factors rather than the Coulomb effect. Moreover, the scatter of experimental values for  $g_{X^0}$  (see, e.g., Ref. [13] for a review of experimental results) is of the same order as the estimated  $g_{X^0}$  renormalization due to Coulomb effect. Based on these arguments we neglect the Coulomb renormalization in our fitting procedure of  $g_{X^0}$  and use the average experimental value  $g_{X^0} = -4$ .

The fitting procedure for the TB model of Ref. [33] results in a good fit of the dispersion of  $c$  and  $v$  bands across high-symmetry paths of the Brillouin zone and only a slight change of energy position and dispersion of high conduction and deep valence bands compared to the original parametrization of Ref. [33]. However this change is sufficient to obtain a large increase of  $|g_{X^0}|$ ,  $g_{X^0} \approx -1.75$  (see column b of Table III). Using the TB model of Ref. [31] we are able to obtain  $g_{X^0} \approx -3.8$  for MoS<sub>2</sub>, WS<sub>2</sub>, and WSe<sub>2</sub> and  $g_{X^0} \approx -2.6$  for MoSe<sub>2</sub> as well as a good fit for all six energy bands dispersions, wave function coefficients, and effective masses, see columns c–f in Table III.

The wide spread of calculated  $g_{X^0}$  values underlies the sensitivity of  $g_{X^0}$  to a given parametrization of a DFT or a TB model. Hence, along with effective masses and energy gaps, the value of  $g_{X^0}$  may serve as a test tool for a given parametrization of a DFT or a TB model.

So far in our theory we treated electron and hole in the exciton independently, neglecting the Coulomb interaction between charge carriers. It is well known, however, that the exciton binding is large in TMDCs and plays a significant role in optical experiments [40,41]. The effects of Coulomb interaction between an electron and a hole as well as localization by an in-plane potential [42] can be estimated by introducing the  $g$ -factor dependence on a charge carrier energy. Such a dependence is derived by simply replacing  $E_c$  with  $E_c + \Delta E_c$  in Eq. (13) and  $E_v$  with  $E_v - \Delta E_v$  in Eq. (14), where  $\Delta E_c$  and  $\Delta E_v$  are the energy shifts of electron and hole levels [43] due to either localization or Coulomb binding. This dependence is depicted in Fig. 2. Note that negative energies  $\Delta E_c, \Delta E_v$  reflect the binding of electron and hole in an exciton, whereas positive  $\Delta E_c, \Delta E_v$  correspond to

localization of a charge carrier in a quantum dot. One can see that within a typical scale of exciton binding energy in TMDCs,  $E_B \sim 400$  meV,  $g_c$  and  $g_v$  change significantly, resulting in a possible enhancement  $\Delta|g_{X^0}| \approx 1$ . However, the detailed calculation of Coulomb correction to  $g_{X^0}$  is beyond the scope of the present work.

## V. CONCLUSIONS

To conclude, we developed a six-band  $k \cdot p$  model that describes the electronic states of monolayer TMDCs in  $\mathbf{K}$  valleys. The set of parameters for the  $k \cdot p$  model is uniquely determined by decomposing 11-band tight-binding models in the vicinity of  $\mathbf{K}^\pm$  points. Using existing in literature TB models we were able to derive systematic parametrizations for different materials (MoS<sub>2</sub>, WS<sub>2</sub>, MoSe<sub>2</sub>, WSe<sub>2</sub>) and different TB Hamiltonians. Using the derived six-band  $k \cdot p$  Hamiltonian we calculated effective masses, Landau levels, and the effective exciton  $g$ -factor  $g_{X^0}$  in different TMDCs. We showed that the main contributions to  $g_{X^0}$  result from the mixing with excited conduction band  $c+2$  and deep valence band  $v-3$ . We also obtained additional sets of  $k \cdot p$  parameters for MoS<sub>2</sub>, WS<sub>2</sub>, MoSe<sub>2</sub>, and WSe<sub>2</sub> by developing our own TB parametrizations based on simultaneous fitting of *ab initio* calculated energy dispersion and the value of  $g_{X^0}$ .

The  $k \cdot p$  parametrizations extracted from existing TB models result in small absolute values of  $g_{X^0}$ , which are far from the experimentally measured  $g_{X^0} \approx -4$ . However, as we showed using our additional sets of  $k \cdot p$  parameters, the change in parameters, which only slightly affects the dispersion of higher conduction and deep valence bands, may result in a significant increase of  $|g_{X^0}|$ . As a result, we obtained  $g_{X^0} \approx -1.75$  and  $g_{X^0} \approx -3.82$  for the two sets, corresponding to MoS<sub>2</sub>,  $g_{X^0} \approx -3.8$  for WS<sub>2</sub> and WSe<sub>2</sub>, and  $g_{X^0} \approx -2.6$  for MoSe<sub>2</sub>. Such a high parameter sensitivity of  $g_{X^0}$  opens a way to further improvement of DFT and TB models, since  $g$ -factor modeling requires at the same time an accurate description of deep valence and high conduction bands.

## ACKNOWLEDGMENTS

I.C.G. thanks the CNRS and the ANR MoS2ValleyControl project for financial support. He also acknowledges the CALMIP initiative for the generous allocation of computational times, through Project p0812, as well as the GENCI-CINES, GENCI-IDRIS, and CINES-CCRT for Grant No. x2016096649. M.V.D. was partially supported by RFBR projects No. 14-02-00168 and No. 16-32-60175, the Russian Federation President Grant No. MK-7389.2016.2, and the Dynasty foundation. The authors acknowledge LIA CNRS-Ioffe RAS ILNACS for financial support. The authors thank M. M. Glazov and T. Amand for fruitful discussions.

## APPENDIX A: PARAMETERS OF $k \cdot p$ MODEL

Parameters of the  $k \cdot p$  Hamiltonians (6) and (7) for different parametrizations, materials, and tight-binding models are listed in Tables IV and V.

TABLE IV. Parameters of the  $k \cdot p$  model as introduced in Eqs. (6) and (7) extracted using the DFT calculations as a starting point. The values of  $\gamma_i$  and  $\delta_i$  are given in eV Å, the units of  $E_i$  are eV, the effective masses  $m'_n$  are given in the units of  $m_0$ . Parametrizations are based on TB models listed in footnotes.

	MoS <sub>2</sub> <sup>a</sup>	MoS <sub>2</sub> <sup>b</sup>	MoSe <sub>2</sub> <sup>b</sup>	WS <sub>2</sub> <sup>b</sup>	WSe <sub>2</sub> <sup>b</sup>
$E_{v-5}$	-6.96	-4.50	-4.42	-5.27	-5.14
$E_{v-4}$	-5.17	-3.83	-3.70	-4.21	-4.02
$E_{v-3}$	-9.59	-3.49	-3.36	-3.82	-3.67
$E_v$	-0.97	-0.03	-0.05	0.04	0.02
$E_c$	0.86	1.77	1.52	2.00	1.69
$E_{c+2}$	1.91	2.98	2.50	3.36	2.80
$\gamma_2$	-5.75	1.62	1.50	1.62	1.49
$\gamma_3$	4.27	3.39	2.96	3.91	3.43
$\gamma_4$	-0.87	-0.92	-0.91	-1.53	-1.44
$\gamma_5$	2.57	-2.66	-2.44	-3.26	-3.04
$\gamma_6$	1.33	0.94	0.84	1.21	1.05
$\delta_1$	3.19	-4.20	-3.86	-4.95	-4.52
$\delta_2$	0.80	-0.19	-0.16	-0.30	-0.29
$\delta_3$	-0.61	2.08	2.11	2.23	2.25
$\delta_4$	-2.05	0.14	-0.06	0.18	-0.06
$\delta_5$	1.74	2.06	1.79	2.15	1.88
$\delta_6$	1.45	0.69	0.48	0.32	0.07
$\delta_7$	7.49	4.45	4.81	4.78	5.14
$m'_{v-5}$	0.87	0.76	0.67	0.64	0.57
$m'_{v-4}$	1.34	0.83	0.78	0.84	0.80
$m'_{v-3}$	6.09	6.92	7.69	9.50	12.32
$m'_v$	-2.81	6.37	6.58	6.64	7.16
$m'_c$	-1.96	-1.16	-1.18	-1.02	-1.04
$m'_{c+2}$	-0.70	-0.60	-0.63	-0.53	-0.55

<sup>a</sup>TB model of Ref. [33] based on DFT calculations.

<sup>b</sup>TB model of Ref. [31] based on DFT calculations.

## APPENDIX B: COMPUTATIONAL DETAILS OF DFT + GW METHOD

The atomic structures and the quasiparticle band structures have been obtained from DFT calculations using the VASP package [44,45]. The Perdew-Burke-Ernzerhof (PBE) [46] functional was used as an approximation of the exchange-correlation electronic term. The software uses the plane-augmented wave scheme [47,48] to treat core electrons. Fourteen electrons for Mo, W atoms and six for S, Se ones are explicitly included in the valence states. All atoms are allowed to relax with a force convergence criterion below 0.005 eV/Å. A grid of  $12 \times 12 \times 1$   $k$  points has been used, in conjunction with a vacuum height of 17 Å, to take benefit of the error's cancellation in the band gap estimates [49]. A Gaussian smearing with a width of 0.05 eV was used for partial occupancies, when a tight electronic minimization tolerance of  $10^{-8}$  eV was set to determine with a good precision the corresponding derivative of the orbitals with respect to  $k$  needed in quasiparticle band structure calculations. Spin-orbit coupling was not included to determine eigenvalues and wave functions as input for the full-frequency-dependent  $GW$  calculations [50] performed at the  $G_0W_0$  level. The total number of states included in the  $GW$  procedure was set to 600,

TABLE V. Parameters of the  $k \cdot p$  model as introduced in Eqs. (6) and (7) extracted using the DFT+ $GW$  calculations as a starting point. The values of  $\gamma_i$  and  $\delta_i$  are given in eV Å, the units of  $E_i$  are eV, the effective masses  $m'_n$  are given in the units of  $m_0$ . Parametrizations are based on TB models listed in footnotes.

	MoS <sub>2</sub> <sup>a</sup>	MoS <sub>2</sub> <sup>b</sup>	MoS <sub>2</sub> <sup>c</sup>	MoSe <sub>2</sub> <sup>c</sup>	WS <sub>2</sub> <sup>c</sup>	WSe <sub>2</sub> <sup>c</sup>
$E_{v-5}$	-4.99	-6.88	-5.20	-5.20	-5.90	-5.79
$E_{v-4}$	-4.32	-4.15	-4.66	-4.62	-4.99	-4.85
$E_{v-3}$	-3.62	-10.52	-4.18	-3.99	-4.39	-4.24
$E_v$	0	0	-0.05	0.00	-0.03	-0.04
$E_c$	2.48	2.47	2.44	2.32	2.98	2.43
$E_{c+2}$	4.04	3.96	4.60	3.95	5.27	4.30
$\gamma_2$	2.08	-8.00	-0.88	-1.50	-1.57	-0.86
$\gamma_3$	4.43	5.93	4.65	4.47	5.41	4.11
$\gamma_4$	-2.14	-1.77	-3.05	-2.65	-3.77	-3.53
$\gamma_5$	-3.07	3.36	-8.27	-6.75	-8.57	-8.37
$\gamma_6$	1.52	1.79	0.67	0.51	0.63	0.40
$\delta_1$	-5.14	4.05	-3.80	-3.98	-5.27	-5.09
$\delta_2$	-0.50	1.26	3.55	3.57	4.18	3.02
$\delta_3$	2.53	0.55	-2.63	-2.35	-1.51	-1.30
$\delta_4$	0.02	-2.09	-0.26	-0.61	-0.54	-0.96
$\delta_5$	2.15	2.28	-0.42	0.14	0.13	-0.71
$\delta_6$	0.69	2.23	-0.23	-0.85	-0.67	-0.05
$\delta_7$	5.05	6.53	3.90	4.31	4.65	4.61
$m'_{v-5}$	0.67	0.85	0.44	0.43	0.41	0.49
$m'_{v-4}$	0.71	2.00	1.22	1.04	1.20	1.01
$m'_{v-3}$	14.00	1.64	0.62	0.70	0.54	0.60
$m'_v$	3.04	-3.39	1.03	1.27	0.96	1.35
$m'_c$	-0.90	-1.33	-0.40	-0.42	-0.37	-0.41
$m'_{c+2}$	-0.47	-0.59	-0.36	-0.40	-0.31	-0.35

<sup>a</sup>TB model of Ref. [31] based on DFT+ $GW$  calculations.

<sup>b</sup>DFT+ $GW$  and TB parametrization of this work (TB model based on Ref. [33]).

<sup>c</sup>DFT+ $GW$  and TB parametrization of this work (TB model based on Ref. [31]).

after a careful check of the direct band gap convergence, to be smaller than 0.1 eV.

### APPENDIX C: DETAILS OF TB FITTING PROCEDURE AND ADDITIONAL TB PARAMETRIZATIONS

Most of the modern TB parametrizations are made to reproduce the energy bands of *ab initio* calculations. The parameter set is usually found by minimizing the error between the DFT and TB energies. We found, however, that even if the parameter set reproduces the electronic bands with great accuracy, it does not necessarily give satisfying values of the  $g$  factor. In order to overcome this problem, we included the calculation of the  $g$  factor in our optimization procedure and varied the TB parameters to fit both the  $GW$  energies and  $g$ -factor values. Within this procedure, the calculated  $g$  factor was obtained via Eqs. (13)–(15) by taking a numerical derivative of the TB Hamiltonian matrix according to Eq. (6). To prevent the order change of the energy bands during optimization we also included the error in the eigenvectors at the  $K$  point. The weights were concentrated in the vicinity of the  $K$  and  $\Gamma$  points of the hexagonal Brillouin zone and had

TABLE VI. Parameters of the TB Hamiltonian (in units of eV) of Ref. [31] obtained after fitting of DFT+ $GW$  calculations.

	MoS <sub>2</sub>	MoSe <sub>2</sub>	WS <sub>2</sub>	WSe <sub>2</sub>
$\epsilon_6$	-0.913	-0.921	-0.755	-0.999
$\epsilon_7$	0.251	0.0117	0.301	-0.047
$\epsilon_8$	0.251	0.0117	0.301	-0.047
$\epsilon_9$	-1.54	-1.62	-1.49	-1.69
$\epsilon_{10}$	-2.26	-2.01	-2.51	-2.25
$\epsilon_{11}$	-2.26	-2.01	-2.51	-2.25
$t_{6,6}^{(1)}$	-0.922	-0.903	-1.02	-0.985
$t_{7,7}^{(1)}$	0.437	0.418	0.622	0.618
$t_{8,8}^{(1)}$	-0.668	-0.658	-0.819	-0.775
$t_{9,9}^{(1)}$	0.24	0.197	0.197	0.191
$t_{10,10}^{(1)}$	1.11	1.24	1.2	1.22
$t_{11,11}^{(1)}$	-0.0029	0.0399	-0.0481	0.028
$t_{6,8}^{(1)}$	0.0462	0.0782	0.121	-0.0083
$t_{9,11}^{(1)}$	-0.0408	-0.206	-0.192	-0.039
$t_{6,7}^{(1)}$	-0.763	-0.705	-0.97	-0.853
$t_{7,8}^{(1)}$	-0.4	-0.347	-0.455	-0.412
$t_{9,10}^{(1)}$	-0.168	-0.15	-0.227	-0.176
$t_{10,11}^{(1)}$	-0.133	-0.14	-0.188	-0.228
$t_{9,6}^{(5)}$	-0.975	-0.816	-0.727	-0.8
$t_{11,6}^{(5)}$	0.0162	0.0554	0.211	0.183
$t_{10,7}^{(5)}$	1.83	1.65	1.99	1.8
$t_{9,8}^{(5)}$	0.914	0.86	0.957	0.811
$t_{11,8}^{(5)}$	-0.0447	-0.115	-0.0814	-0.0766
$t_{9,6}^{(6)}$	0.936	0.793	1.13	0.993
$t_{11,6}^{(6)}$	0.945	0.857	0.906	0.728
$t_{9,8}^{(6)}$	0.797	0.702	0.985	0.888
$t_{11,8}^{(6)}$	0.449	0.343	0.493	0.31

higher values for  $v$  and  $c$  bands for better reproduction of the most important electronic states.

The parameter optimization was thus carried out by minimizing the function

$$\begin{aligned}
 f(\{t_i\}) = & \sum_{i,k} w_{i,k} (E_{i,k}^{\text{TB}} - E_{i,k}^{\text{GW}})^2 \\
 & + \sum_i u_i [(C_{i,\Gamma}^{\text{TB}} - C_{i,\Gamma}^{\text{GW}})^2 + (C_{i,K}^{\text{TB}} - C_{i,K}^{\text{GW}})^2] \\
 & + v (g_{X^0}^{\text{TB}} - g_{X^0}^{\text{expt}})^2, \quad (\text{C1})
 \end{aligned}$$

where  $\{t_i\}$  are the TB parameters,  $i$  and  $k$  denote the number of the electronic band and the wave vector, respectively, and  $w_{i,k}$ ,  $u_i$ , and  $v$  are the weight coefficients. In Eq. (C1)  $E_i^{\text{TB}}$  and  $C_i^{\text{TB}}$  are the tight-binding energies and coefficients of wave functions decomposition, which depend on the particular TB Hamiltonian and parameters used, and  $E_i^{\text{GW}}$  and  $C_i^{\text{GW}}$  are the values, obtained by DFT+ $GW$  or another *ab initio* method.

TABLE VII. Parameters of the TB Hamiltonian (in units of eV) of Ref. [33] for MoS<sub>2</sub> obtained after fitting of DFT+GW calculations.

$\epsilon_0$	$\epsilon_2$	$\epsilon_p$	$\epsilon_z$	$V_{pd\sigma}$	$V_{pd\pi}$	$V_{dd\sigma}$
-5.707	-5.784	-8.319	-12.171	4.791	-1.606	-1.221
$V_{dd\pi}$	$V_{dd\sigma}$	$V_{pp\sigma}$	$V_{pp\pi}$			
0.526	0.359	0.905	-0.396			

Parameter  $g_{X^0}^{\text{TB}}$  is the  $g$ -factor value calculated according to Eqs. (13)–(15) from the TB Hamiltonian, and  $g_{X^0}^{\text{expt}}$  is the experimental value. The fitting was carried out by a random search algorithm until a compromise between the quality of the band structure and  $g$ -factor value for MoS<sub>2</sub>, MoSe<sub>2</sub>, WS<sub>2</sub>, and WSe<sub>2</sub> was found.

Resulting parametrizations of TB Hamiltonians of Refs. [31] (for MoS<sub>2</sub>, MoSe<sub>2</sub>, WS<sub>2</sub>, and WSe<sub>2</sub>) and [33] (for MoS<sub>2</sub>) are presented in Tables VI and VII. The resulting energy dispersions in comparison with DFT+GW calculations for MoS<sub>2</sub> are presented in Fig. 3. Based on these two sets of TB parameters we obtained  $k \cdot p$  parametrizations listed in Table V, columns b–f, with effective masses and  $g$  factor listed in Table III, columns b–f.

#### APPENDIX D: LANDAU LEVELS

The developed  $k \cdot p$  model allows for calculation of Landau levels in the system. For this purpose we make replacements  $q_+ \rightarrow \sqrt{2}a^\dagger/l_B$  and  $q_- \rightarrow \sqrt{2}a/l_B$  in Eqs. (6) and (7), where  $a^\dagger$  and  $a$  are the creation and annihilation operators acting in the space of Landau functions  $l_B = \sqrt{|e|\hbar|B_z|}c$ , and decompose the six-component wave function of the  $j$ th band  $\Psi^{(j)}$  in a

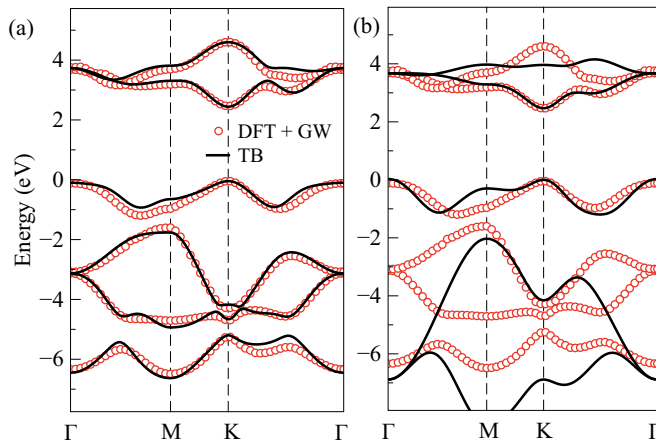


FIG. 3. DFT+GW and TB calculations for electronic energy dispersion in MoS<sub>2</sub>. (a) The fit of TB model of Ref. [31] and (b) the fit of TB model of Ref. [33]. The zero energy was aligned to the top of the valence band  $v$ .

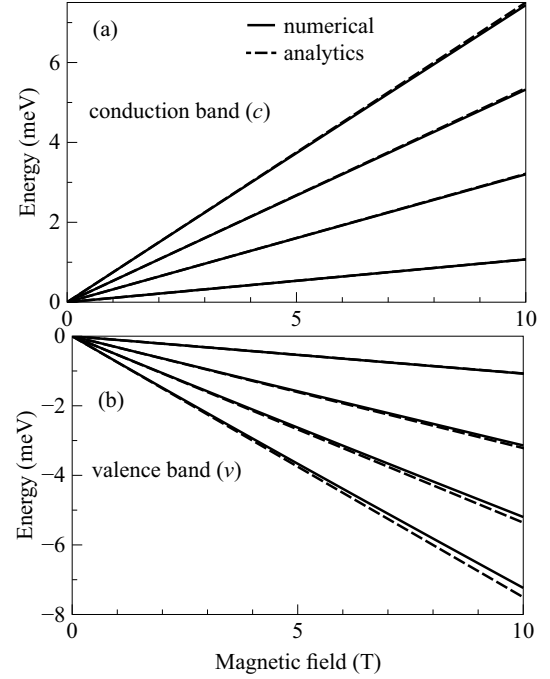


FIG. 4. Dispersion of the first four Landau levels in the bottom conduction ( $c$ ) and topmost valence ( $v$ ) bands calculated using parametrization (a) of the  $k \cdot p$  model (see Table IV). Solid lines show the results of numeric calculations using decomposition Eq. (D1), and dashed lines stand for a simple analytical formula  $\epsilon_j(n, B_z) = \hbar\omega_c^{(j)}(n + 1/2)$  (see text for details).

series of the Landau level functions  $\varphi_{n, q_y}$  [51],

$$\Psi^{(j)} = \sum_{n \geq 0} \begin{pmatrix} a_n \\ b_n \\ c_n \\ d_n \\ e_n \\ f_n \end{pmatrix} \varphi_{n, q_y}, \quad (\text{D1})$$

where  $n$  and  $q_y$  are the quantum numbers, and  $a_n$ ,  $b_n$ ,  $c_n$ ,  $d_n$ ,  $e_n$ , and  $f_n$  are coefficients. The numeric diagonalization of obtained Hamiltonian yields the energy position of the  $j$ th band in magnetic field  $E_j(n, B_z)$ . However, this energy contains also the valley Zeeman term, described by the second term of Eq. (11). To get rid of the Zeeman term we define Landau levels as  $\epsilon_j(n, B_z) = 1/2[E_j(n, B_z) + E_j(n, -B_z)]$ .

The dispersion of the first four Landau levels for  $j = c$  and  $j = v$  is presented in Fig. 4. For comparison we also show linear dispersions calculated using the simple formula  $\epsilon_j(n, B_z) = \hbar\omega_c^{(j)}(n + 1/2)$ , with  $\omega_c^{(j)} = |eB_z|/m_jc$  and the effective masses  $m_c$  and  $m_v$  given by Eq. (8). One can see that the results given by the exact numeric diagonalization of the effective Hamiltonian and the simple analytical formula coincide in the wide range of  $B_z$ , the discrepancy in the valence band is more noticeable due to more pronounced band nonparabolicity.

- [1] K. F. Mak, C. Lee, J. Hone, J. Shan, and T. F. Heinz, *Phys. Rev. Lett.* **105**, 136805 (2010).
- [2] Q. H. Wang, K. Kalantar-Zadeh, A. Kis, J. N. Coleman, and M. S. Strano, *Nat. Nano* **7**, 699 (2012).
- [3] D. Xiao, G.-B. Liu, W. Feng, X. Xu, and W. Yao, *Phys. Rev. Lett.* **108**, 196802 (2012).
- [4] K. F. Mak, K. He, J. Shan, and T. F. Heinz, *Nat. Nano* **7**, 494 (2012).
- [5] T. Cao, G. Wang, W. Han, H. Ye, C. Zhu, J. Shi, Q. Niu, P. Tan, E. Wang, B. Liu, and J. Feng, *Nat. Commun.* **3**, 887 (2012).
- [6] G. Sallen, L. Bouet, X. Marie, G. Wang, C. R. Zhu, W. P. Han, Y. Lu, P. H. Tan, T. Amand, B. L. Liu, and B. Urbaszek, *Phys. Rev. B* **86**, 081301 (2012).
- [7] Y. Li, J. Ludwig, T. Low, A. Chernikov, X. Cui, G. Arefe, Y. D. Kim, A. M. van der Zande, A. Rigosi, H. M. Hill, S. H. Kim, J. Hone, Z. Li, D. Smirnov, and T. F. Heinz, *Phys. Rev. Lett.* **113**, 266804 (2014).
- [8] D. MacNeill, C. Heikes, K. F. Mak, Z. Anderson, A. Kormányos, V. Zólyomi, J. Park, and D. C. Ralph, *Phys. Rev. Lett.* **114**, 037401 (2015).
- [9] A. Srivastava, M. Sidler, A. V. Allain, D. S. Lembke, A. Kis, and A. Imamoglu, *Nat. Phys.* **11**, 141 (2015).
- [10] G. Aivazian, Z. Gong, A. M. Jones, R.-L. Chu, J. Yan, D. G. Mandrus, C. Zhang, D. Cobden, W. Yao, and X. Xu, *Nat. Phys.* **11**, 148 (2015).
- [11] G. Wang, L. Bouet, M. M. Glazov, T. Amand, E. L. Ivchenko, E. Palleau, X. Marie, and B. Urbaszek, *2D Mater.* **2**, 034002 (2015).
- [12] A. A. Mitioglu, P. Plochocka, Á. Granados del Aguila, P. C. M. Christianen, G. Deligeorgis, S. Anghel, L. Kulyuk, and D. K. Maude, *Nano Lett.* **15**, 4387 (2015).
- [13] A. V. Stier, K. M. McCreary, B. T. Jonker, J. Kono, and S. A. Crooker, *Nat. Commun.* **7**, 10643 (2016).
- [14] A. A. Mitioglu, K. Galkowski, A. Surrente, L. Klotkowski, D. Dumcenco, A. Kis, D. K. Maude, and P. Plochocka, *Phys. Rev. B* **93**, 165412 (2016).
- [15] A. Arora, R. Schmidt, R. Schneider, M. R. Molas, I. Breslavetz, M. Potemski, and R. Bratschitsch, *Nano Lett.* **16**, 3624 (2016).
- [16] A. Kormányos, P. Rakyta, and G. Burkard, *New J. Phys.* **17**, 103006 (2015).
- [17] R.-L. Chu, X. Li, S. Wu, Q. Niu, W. Yao, X. Xu, and C. Zhang, *Phys. Rev. B* **90**, 045427 (2014).
- [18] H. Rostami and R. Asgari, *Phys. Rev. B* **91**, 075433 (2015).
- [19] E. L. Ivchenko and G. E. Pikus, *Superlattices and Other Heterostructures* (Springer, Berlin, 1997).
- [20] L. C. L. Y. Voon and M. Willatzen, *The  $kp$  Method: Electronic Properties of Semiconductors* (Springer, Berlin, 2009).
- [21] G. Pikus, V. Maruschak, and A. Titkov, *Sov. Phys. Semicond.* **22**, 115 (1988).
- [22] I. Vurgaftman, J. R. Meyer, and L. R. Ram-Mohan, *J. Appl. Phys.* **89**, 5815 (2001).
- [23] J.-M. Jancu, R. Scholz, E. A. de Andrada e Silva, and G. C. La Rocca, *Phys. Rev. B* **72**, 193201 (2005).
- [24] M. V. Durnev, M. M. Glazov, and E. L. Ivchenko, *Phys. Rev. B* **89**, 075430 (2014).
- [25] A. Kormányos, G. Burkard, M. Gmitra, J. Fabian, V. Zólyomi, N. D. Drummond, and V. Fal'ko, *2D Mater.* **2**, 022001 (2015).
- [26] A. Kormányos, V. Zólyomi, N. D. Drummond, and G. Burkard, *Phys. Rev. X* **4**, 011034 (2014).
- [27] A. Kormányos, V. Zólyomi, N. D. Drummond, P. Rakyta, G. Burkard, and V. I. Fal'ko, *Phys. Rev. B* **88**, 045416 (2013).
- [28] C. Hermann and C. Weisbush, *Optical Orientation*, edited by F. Meier and B. Zakharchenya (North-Holland, Amsterdam, 1984).
- [29] E. Cappelluti, R. Roldán, J. A. Silva-Guillén, P. Ordejón, and F. Guinea, *Phys. Rev. B* **88**, 075409 (2013).
- [30] R. Roldán, M. P. López-Sancho, F. Guinea, E. Cappelluti, J. A. Silva-Guillén, and P. Ordejón, *2D Mater.* **1**, 034003 (2014).
- [31] S. Fang, R. Kuate Defo, S. N. Shirodkar, S. Lieu, G. A. Tritsarlis, and E. Kaxiras, *Phys. Rev. B* **92**, 205108 (2015).
- [32] E. Ridolfi, D. Le, T. S. Rahman, E. R. Mucciolo, and C. H. Lewenkopf, *J. Phys.: Condens. Matter* **27**, 365501 (2015).
- [33] H. Rostami, R. Roldán, E. Cappelluti, R. Asgari, and F. Guinea, *Phys. Rev. B* **92**, 195402 (2015).
- [34] A. Molina-Sánchez, K. Hummer, and L. Wirtz, *Surf. Sci. Rep.* **70**, 554 (2015).
- [35] A. Molina-Sánchez, P. Sangalli, K. Hummer, A. Marini, and L. Wirtz, *Phys. Rev. B* **88**, 045412 (2013).
- [36] H. Shi, H. Pan, Y.-W. Zhang, and B. I. Yakobson, *Phys. Rev. B* **87**, 155304 (2013).
- [37] Note that this rule depends on the choice of the wave functions phase, i.e., in Ref. [25]  $q_{\pm} \rightarrow -q_{\mp}$ .
- [38] T. Eknapakul, P. D. C. King, M. Asakawa, P. Buaphet, R.-H. He, S.-K. Mo, H. Takagi, K. M. Shen, F. Baumberger, T. Sasagawa, S. Junghwan, and W. Meevasana, *Nano Lett.* **14**, 1312 (2014).
- [39] M. M. Glazov, E. L. Ivchenko, G. Wang, T. Amand, X. Marie, B. Urbaszek, and B. L. Liu, *Phys. Status Solidi B* **252**, 2349 (2015).
- [40] K. He, N. Kumar, L. Zhao, Z. Wang, K. F. Mak, H. Zhao, and J. Shan, *Phys. Rev. Lett.* **113**, 026803 (2014).
- [41] A. Chernikov, T. C. Berkelbach, H. M. Hill, A. Rigosi, Y. Li, O. B. Aslan, D. R. Reichman, M. S. Hybertsen, and T. F. Heinz, *Phys. Rev. Lett.* **113**, 076802 (2014).
- [42] A. Branny, G. Wang, S. Kumar, C. Robert, B. Lassagne, X. Marie, B. D. Gerardot, and B. Urbaszek, *Appl. Phys. Lett.* **108**, 142101 (2016).
- [43] E. L. Ivchenko, *Optical Spectroscopy of Semiconductor Nanostructures* (Alpha Science, Harrow, UK, 2005).
- [44] G. Kresse and J. Hafner, *Phys. Rev. B* **47**, 558(R) (1993).
- [45] G. Kresse and J. Furthmüller, *Phys. Rev. B* **54**, 11169 (1996).
- [46] J. P. Perdew, K. Burke, and M. Ernzerhof, *Phys. Rev. Lett.* **77**, 3865 (1996).
- [47] P. E. Blöchl, *Phys. Rev. B* **50**, 17953 (1994).
- [48] G. Kresse and D. Joubert, *Phys. Rev. B* **59**, 1758 (1999).
- [49] F. Hüser, T. Olsen, and K. S. Thygesen, *Phys. Rev. B* **88**, 245309 (2013).
- [50] M. Shishkin and G. Kresse, *Phys. Rev. B* **74**, 035101 (2006).
- [51] E. I. Rashba, *Fiz. Tverd. Tela* **2**, 1874 (1964) [*Sov. Phys. Solid State* **2**, 1109 (1960)].